Appl Phys A (2009) 94: 247–251
DOI 10.1007/s00339-008-4765-y

Applied Physics A
Materials Science & Processing

Thermal stability of catalytically grown multi-walled carbon nanotubes observed in transmission electron microscopy

Cheng-Yu Wang · Chuan-Pu Liu · C.B. Boothroyd

Received: 15 November 2007 / Accepted: 3 June 2008 / Published online: 4 July 2008

Abstract The thermal stability of multi-walled carbon nanotubes (MWCNTs) was assessed in situ by transmission electron microscopy. Upon heating, Ni catalysts in MWCNTs containing bamboo structures shrank from the tail due to evaporation, leading to additional bamboo formation and tube elongation at 800°C, while the MWCNTs with FeSi catalysts remained intact up to 1050°C except for better crystallinity. The physisorbed carbon and/or hydrocarbon on surfaces and super-saturated carbon in the Ni catalysts should be responsible for the phenomena.

PACS 81.01.De · 81.07.Bc · 87.64.Ee

1 Introduction

Carbon nanotubes (CNTs) have stimulated great research interest since their first report in 1991 [1], for their unique conformations to be ideal quantum wires and because they can act as the building blocks for nanoscale devices due to their intrinsically metallic and semi-conductive properties, which are determined by their diameter and chirality [2, 3]. They have been applied in field emission and vacuum microelectronics, high sensitive sensors and probes [4].

Although CNTs have been synthesized by many methods, catalytic growth with chemical vapor deposition (CVD) could significantly lower the reaction temperature and exhibit the potential to generate high density and well-aligned CNTs [5]. The CVD techniques that allow for bulk production of nanotube films have also been developed with an increasing ability to control the uniformity and the properties of the products [6]. Nucleation of carbon filaments with catalysts have been systematically analyzed in terms of the Gibbs free energy, and the calculations reveal that both carbon supersaturation in the metal particles and the state of the metal particles affect the stable size of a nucleus [7]. However, systems containing eutectic reactions, such as Fe–, Ni– and Co–C, would need more, both theoretical and experimental, studies, for the metal particles transforming into liquid, and the state favors growing SWCNTs according to the same report [7]. On the other hands, root- or tip-growth mechanisms [8–12] have been proposed to explain the growth of CNTs. Nevertheless, further growth improvement still requires a deeper understanding of the entire catalytic growth process. Besides, the further implementation of CNT nanodevices also demands not only the understanding of CNT handling and assembly but also the assessment of the thermal stability of CNTs, since devices would experience heating during the fabrication process.

In-situ transmission electron microscopy (TEM) can be applied to closely monitor the growth and reaction processes in real time and thus has been successfully applied to examine some growth issues of CNTs. For example, the entire CNT growth in the early stage has been demonstrated, including the occurrence of the first spheroidal carbon layer from a catalyst to the necking of spheroidal particles [13]. Catalyst dynamics has been examined for the nu-

C.-Y. Wang
Department of Materials Science and Engineering, National Cheng Kung University, Tainan 701, Taiwan

C.-P. Liu (✉)
Center for Micro/Nano Science and Technology, National Cheng Kung University, Tainan 701, Taiwan
e-mail: cpliu@mail.ncku.edu.tw

C.B. Boothroyd
Center for Electron Nanoscopy, Technical University of Denmark, 2800 Kongens Lyngby, Denmark

cleation of surface-bound single-walled CNTs and carbon nanofibers [14]. Ni particles on a MgO substrate [15, 16] and on a SiO_x coated TEM grid [14] have been found to remain metallic and crystalline during CNT growth. Intense electron beam irradiation and heating could transform rod-like carbon into CNTs [17]. Moreover, the crystallinity of multi-walled graphene sheets could be improved by similar effects [18].

In this paper, we report on the dynamical structure evolution of multi-walled CNTs (MWCNTs) upon annealing. Depending on the type of catalyst used, the evolution of the structure may include bamboo structure formation and tube elongation in an externally carbon-free environment. The proposed mechanism responsible for the structure changes provides direct evidence for the tip-growth mechanism. This study also provides useful information on catalyst removal and the opening of MWCNTs by vacuum heating, which enables purer MWCNTs, in contrast to wet chemistry [19].

2 Method

Two types of MWCNTS were prepared for this study. The first type was produced by induced couple plasma CVD (ICP-CVD) using Ni as the catalyst. The second type was synthesized by microwave power enhanced CVD (MPE-CVD) using FeSi as the catalyst. For detailed experimental procedures for these original materials one is referred to the literature [20, 21]. The in-situ experiments were performed in a JEOL-2000V TEM under ultra-high vacuum (UHV) with a base pressure of about 1×10^{-9} Torr. The UHV TEM was operated at 200 keV and was equipped with a LaB_6 gun, a charge coupled device (CCD) camera and a Gatan imaging filter (GIF) system. Some of the post-analyses were also performed in a JEOL2100F TEM, operated at 200 keV, fitted with a field emission gun, a CCD and a GIF system. The as-grown CNTs were scraped off from the substrate and dipped in acetone for good dispersion and then dropped onto a TEM molybdenum (Mo) grid. This grid was baked dry, glued onto a Si substrate that served as the ohmic heating source prior to loading into the TEM. The experiments were recorded on video at TV scan rate. The temperature reading was deduced from the current supplied to the heater, which had previously been calibrated using an optical pyrometer. The heating was performed in stages with the temperature held at several values starting from 400°C for about 10 minutes each.

3 Experimental results and discussion

Bright field (BF) and high-resolution TEM (HR-TEM) images of the as-grown MWCNTs by ICP-CVD are shown in Fig. 1. According to Fig. 1a with the corresponding diffraction pattern (DP) in the inset, the as-grown MWCNT is

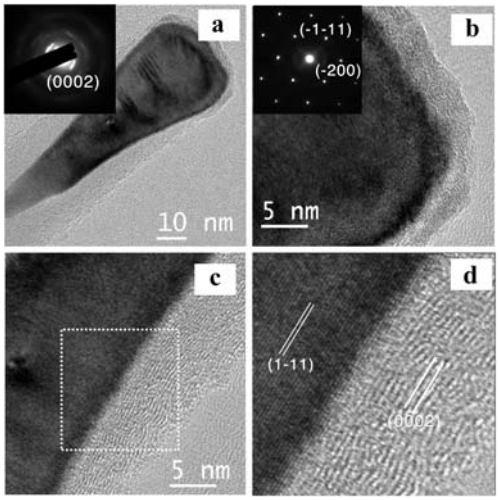

Fig. 1 HRTEM images showing (**a**) the morphology of the tip of an as-grown ICP-CVD CNT with a conical Ni nanocrystal, where the inset is the DP of the CNT, (**b**) amorphous carbon and/or hydrocarbon residue coated on the catalyst surface, with the inset for the DP of the Ni crystal, (**c**) better crystalline graphene walls near the tail of the Ni nanocrystal, with (**d**) a close-up image from the area marked in (**c**) revealing the lattice fringes from the catalyst to the graphene walls

crystalline with defects, consisting of multi-walled graphene sheets, which produce (0002) spots in the DP, and a conical catalytic particle at the tip. The catalyst was wrapped with crystalline graphene sheets and a thin layer of amorphous carbon and/or hydrocarbon residue on top, in Fig. 1b. According to the DP in the inset of Fig. 1b, the catalyst is face-centered cubic phase with a {111} spacing of 0.208 nm and a (200) spacing of 0.175 nm, all of which are larger than those of Ni, 0.199 nm and of 0.172 nm, respectively, from JCPDS [22]. The enlarged lattice parameters should result from carbon solid solution in Ni, but apparently the alloy particles did not convert to nickel carbide during growth or rapid cooling after the CVD process [15, 23, 24].

Upon heating, the ICP-CVD MWCNTs sequentially underwent a reaction pathway, and snapshots at different temperature were reproduced from a MWCNT, vertically aligned with respect to that of 450°C, as shown in Fig. 2. The catalyst started shrinking from 575°C, while still remaining crystalline until 800°C, after which a small liquid particle was left at the tip of the CNT in Fig. 2e. Two additional bamboo structures formed at the innermost shell on the way when the catalyst retreated, as indicated in Fig. 2e. Between the two compartments, a step was also observed in Fig. 2e. The newly formed bamboo structures were attributed to the carbon atoms originally dissolved in the catalyst during synthesis and segregated when the catalyst shrank. Another possible carbon source resulted from thermal activation of the thin amorphous carbon and/or hydrocarbon layer wrapping the catalytic particle on top. A similar growth mechanism has been reported previously [25, 26], but initial crystal structures of the raw materials determined whether the

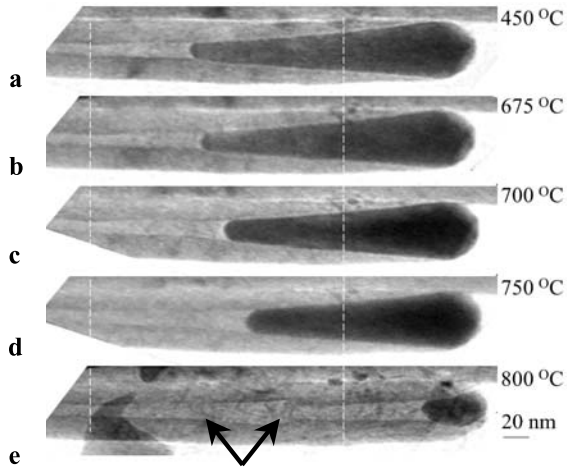

Fig. 2 Snapshots of dynamical observations of a ICP-CVD CNT upon heating from 450°C to 800°C. Two *reference lines* are marked for easier comparison of the length extension. The *arrows* indicate the positions of newly formed bamboo structures

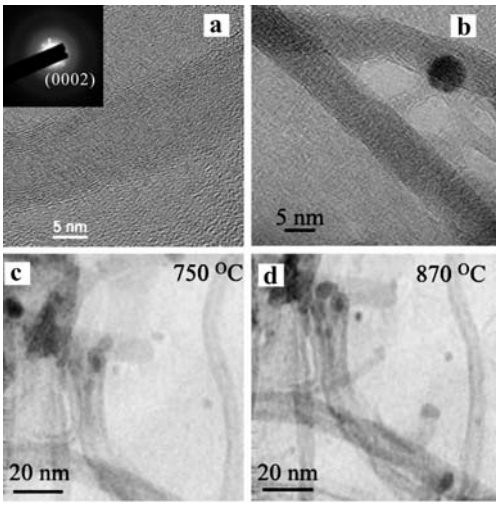

Fig. 3 TEM images showing the morphologies of MPE-CVD CNTs (**a**) before and (**b**) after heating, where the inset in (**a**) is the DP of the tube, with two snapshots from a video reproduced at (**c**) 750°C and (**d**) 870°C during heating

carbon segregation process would undergo tubulization of amorphous rods [25] or growth of new shells from the innermost wall of a defective tube [26]. Furthermore, the tube length was also measured from the snapshots in Fig. 2. There are two white lines drawn between the snapshots for easier comparison. The reference line on the left marks an extrusion point at the innermost shell which was aligned, while that on the right marks the position of a tiny particle adhering to the outer most shell in the image at 450°C. Clearly this particle was displaced to the right of the reference line as the temperature increased. On measuring the length change, the MWCNT experiences an elongation of 4 nm at 750°C and 17 nm at 800°C. The diameter of the CNT remains about 48 nm throughout the entire heating process. The extra carbon source causing the tube elongation may resort to the same as for the formation of the additional bamboo structures.

Moving on to the as-grown MPE-CVD CNTs: these exhibit multi-walled features as shown in Fig. 3a with the inset for the DP of the tube. The less perfect (0002) spots may reflect the imperfection of the tubes and are partially caused by electron irradiation. The onion-like graphene shells entirely encapsulated the FeSi nanoparticles located at the tip. Two snapshots from the video of the MWCNT during heating at 750°C and 870°C are shown in Fig. 3c and d. These lower magnification images were taken to allow for the observations of the entire MWCNT. Throughout the entire heating process, the MWCNTs were fairly stable when compared to the previous sample, and no obvious tube variations were observed. However, an HR-TEM analysis of a typical MWCNT after heating, shown in Fig. 3b, reveals that the walls of the CNT become straighter, indicating that structural defects were annihilated by annealing. Therefore, the contraction of the catalyst and elongation of a CNT upon heating must be related to the material of the catalyst used and the morphology of the as-grown MWCNTs.

The experimental atmosphere in the microscope was the same for both samples where there exist only negligible sources of carbon due to the use of a carbon-coated Mo grid. The difference between the Ni and Fe–Si nanoparticles embedded in the MWCNTs is that the Ni nanoparticle exhibits an uncapped conical top with a long conical tail and a better epitaxial interface with the shells of CNTs, whereas the Fe–Si nanoparticle exhibits a spherical shape and becomes completely encapsulated by the graphene shells. Therefore, the open end of the Ni nanoparticle should be responsible for the nanoparticle shrinkage, bamboo structures formation and tube length extension. However, the first question to discuss is where the carbon came from. The common growth mechanism proposed that carbon atoms in the precursors were first dissolved in the catalysts to form an supersaturated solid solution, from which carbon then segregated to grow a CNT. Therefore, the Ni catalyst should contain carbon when the growth process terminated. This dissolved carbon segregated on the surface when the catalyst shrank, and carbon could also be continuously supplied from the top surface of the catalyst, which adsorbed a thin layer of amorphous carbon and/or hydrocarbon layer. The continuation of the MWCNT growth upon annealing in this case is consistent with the tip-growth mechanism of the nanotubes, found previously by scanning electron microscopy [20].

The Ni {111} planes correlate closely to the graphene (0002) planes, namely the epitaxial interface. Crystalline Ni nanoparticles have been shown to catalytically synthesize MWCNTs at 536°C [24]. Our results reveal that the Ni catalyst melts at about 780°C and the evaporated atoms

rapidly diffuse out of the tip of the CNT, leaving behind a small particle, as shown in Fig. 2e. According to Ni–C phase diagram [27], the melting temperature (T_m) of pure Ni is 1450°C and the eutectic temperature is 1326°C. These temperatures are far higher than the experimentally observed temperature of 780°C. Size dependent melting of nanocrystals constrained in CNTs needs to be considered. Following the treatment by Jiang et al. [28], T_m will be reduced by 186°C for a conical shaped Ni particle, where the radius is taken by averaging the diameter at the tail, 12 nm, and the top, 48 nm, of the catalyst. If allowing for carbon dissolving in interstitial sites of Ni, the T_m can be further reduced by 173°C, down to 1153°C, which is still higher than 780°C. Curled graphene networks produce a compressive field [26], which in turn would increase T_m but could be released by rapid diffusion and/or evaporation of Ni as temperature increases. The large discrepancy may be further contributed to by the interaction between the graphene shells and the surface layer of the Ni catalyst, which needs further analysis.

On the other hand, the MWCNTs containing FeSi catalysts remain intact throughout the entire annealing, except that the FeSi catalysts underwent the solid-liquid transition at 850°C, where the catalysts become spherical in shape. The carbon concentration in the catalyst has been estimated to be 12 at.% [21], which renders T_m to be about 1260°C according to Fe–C–Si phase diagram [27]. The size effect will reduce T_m to 668°C by 592°C for a nanoparticle of 3 nm, which is lower than 850°C. A plausible explanation is that this temperature reduction can be compensated for by the constrained stress exerted by onion-like shells.

The whole pathway for Ni nanoparticle synthesizing CNTs during annealing is depicted in Fig. 4. The as-grown CNT contains a Ni nanocrystal embedded at the tip, wrapped by graphene shells and a thin amorphous carbon and/or hydrocarbon layer in Fig. 4a. The thermally activated thin amorphous carbon and/or hydrocarbon layer dissolves into Ni nanoparticles as temperature increases; see Fig. 4b. The graphene shells of the bamboo structures segregate from the tail of the Ni nanoparticle and take the shape of the catalyst. Continuous shrinkage due to evaporation results in graphene shells segregating from a Ni catalyst; see Fig. 4c. The crystalline Ni catalyst becomes liquid phase at 780°C, Fig. 4d, accompanied by the formation of graphene shells of the same bamboo structure at a temperature higher than 780°C. The liquid phase assists the catalyst splitting from the graphene shells, following the similar step in Fig. 4c.

The observation favors the tip-growth mechanism for the MWCNTs synthesized with Ni as the catalyst compared with the SEM results in [20]. The FeSi catalysts were fully encapsulated in CNTs and hence there was no free surface for physical absorption and no low energy diffusion path for further tube growth. Nevertheless, the crystallinity of the shells became better after heating, consistent with previous observations [29, 30].

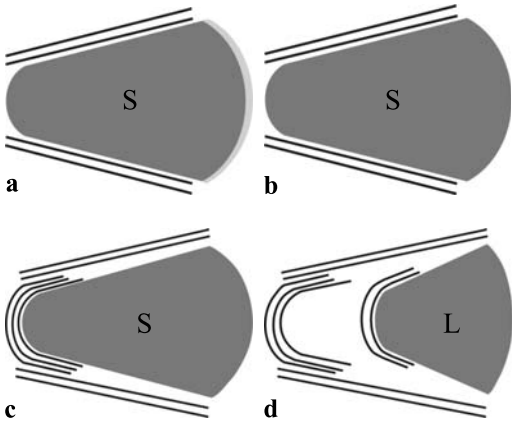

Fig. 4 Schematic diagrams illustrating the steps of the bamboo structure formation for a MWCNT containing a Ni catalyst on the tip upon heating. (**a**) An as-grown CNT and (**b**) carbon and/or hydrocarbon residue at the surface dissolved into Ni, (**c**) the segregation of graphene shells from the Ni catalyst and (**d**) bamboo structures clearly observed after graphene-particle splitting

4 Conclusions

Upon annealing in a UHV-TEM, we observe that MWCNTs with uncapped Ni catalysts at their tips exhibit a series of structural evolution steps including additional bamboo structures formation as the catalyst evaporates and the tube elongates. However, MWCNTs with fully encapsulated catalysts at onion-like tips only underwent structure healing on heating. The proposed mechanism for the structure changes is consistent with the tip-growth mode for MWCNTs grown by using Ni as the catalysts [20] and the easier removement of such catalyst from MWCNTs. CNTs may act as ideal nanoscale pressure cells causing the melting temperature of the nanocrystals, constrained inside, greatly reduced compared to the Ni case.

Acknowledgements This project was supported by the National Science Counsel, Taiwan under grant contract number NSC 92-2120-E-006-003 through an international collaboration program with IMRE, Singapore. We sincerely thank Prof. Hong and Prof. Ting in the department of Materials Science and Engineering of National Cheng Kung University for providing the CNTs analyzed here as well as the center for Micro/Nano science and technology, National Cheng Kung University, Taiwan, for equipment access and technical support. We would also like to thank Dr. Foo and Dr. Lin for their help with the in-situ microscopy at IMRE.

References

1. S. Iijima, Nature **354**, 56 (1991)
2. J.W.G. Wildöer, L.C. Venema, A.G. Rinzler, R.E. Smalley, C. Dekker, Nature **391**, 59 (1998)
3. T.W. Odom, J.L. Huang, P. Kim, C.M. Lieber, Nature **391**, 62 (1998)
4. R.H. Baughman, A.A. Zakhidov, W.A. de Heer, Science **297**, 787 (2002)

5. C. Bower, W. Zhu, S. Jin, O. Zhou, Appl. Phys. Lett. **77**, 830 (2000)
6. K. Hata, D.N. Futaba, K. Mizuno, T. Namai, M. Yumura, S. Iijima, Science **306**, 1362 (2004)
7. V.L. Kuznetsov, A.N. Usoltseva, A.L. Chuvilin, Phys. Rev. B **64**, 235401 (2001)
8. L.P. Biró, G. Molnár, I. Szabó, Z. Vértesy, Z.E. Horváth, J. Gyulai, Z. Kónya, P. Piedigrosso, A. Fonseca, J.B. Nagy, P.A. Thiry, Appl. Phys. Lett. **76**, 706 (2000)
9. C. Bower, O. Zhou, W. Zhu, D.J. Werder, S. Jin, Appl. Phys. Lett. **77**, 2767 (2000)
10. C.J. Lee, J. Park, Appl. Phys. Lett. **77**, 3397 (2000)
11. M. Okai, T. Muneyoshi, T. Yaguchi, S. Sasaki, Appl. Phys. Lett. **77**, 3468 (2000)
12. L.C. Chen, C.Y. Wen, C.H. Liang, W.K. Hong, K.J. Chen, H.C. Cheng, C.S. Chen, C.T. Wu, K.H. Chen, Adv. Funct. Mater. **12**, 687 (2002)
13. H. Watanabe, Y. Hisada, S. Mukainakano, N. Tanaka, J. Microsc. **203**, 40 (2001)
14. S. Hofmann, R. Sharma, C. Ducati, G. Du, C. Mattevi, C. Cepek, M. Cantoro, S. Pisana, A. Parvez, F. Cervantes-Sodi, A. Ferari, R. Dunin-Borkowski, S. Lizzit, L. Petaccia, A. Goldoni, J. Robertson, Nano Lett. **7**, 602 (2007)
15. M. Lin, J.P.Y. Tan, C. Boothroyd, K.P. Loh, E.S. Tok, Y.L. Foo, Nano Lett. **6**, 449 (2006)
16. M. Lin, J.P.Y. Tan, C. Boothroyd, K.P. Loh, E.S. Tok, Y.L. Foo, Nano Lett. **7**, 2234 (2007)
17. A. Yasuda, N. Kawase, W. Mizutani, J. Phys. Chem. B **106**, 13294 (2002)
18. F. Banhart, Rep. Prog. Phys. **62**, 1181 (1999)
19. A.C. Dillon, T. Genett, K.M. Jones, J.L. Alleman, P.A. Parilla, M.J. Heben, Adv. Mater. **11**, 1354 (1999)
20. J.H. Yen, I.C. Leu, C.C. Lin, M.H. Hon, Appl. Phys. A **80**, 415 (2005)
21. J.M. Ting, K.H. Liao, Chem. Phys. Lett. **396**, 469 (2004)
22. J. Haglund, A.F. Guillermet, G. Grimvall, M. Korling, Phys. Rev. B **48**, 11685 (1993). JCPDS No. 88-2326
23. C. Ducati, I. Alexandrou, M. Chhowalla, J. Robertson, G.A.J. Amaratunga, J. Appl. Phys. **95**, 6387 (2004)
24. S. Helveg, C. López-Cartes, J. Sehested, P.L. Hansen, B.S. Clausen, J.R. Rostrup-Nielsen, F. Abild-Pedersen, J.K. Norskov, Nature **427**, 426 (2004)
25. T. Ichihashi, J. Fujita, M. Ishida, Y. Ochiai, Phys. Rev. Lett. **92**, 215702 (2004)
26. L. Sun, F. Banhart, A.V. Krasheninnikov, J.A. Rodriguez-Manzo, M. Terrones, P.M. Ajayan, Science **312**, 1199 (2006)
27. H. Baker (ed.), *Alloy Phase Diagram*. ASM Handbook, vol. 3 (ASM International, Materials Park, 1992)
28. Q. Jiang, N. Aya, F.G. Shi, Appl. Phys. A **64**, 627 (1997)
29. F. Banhart, J. Appl. Phys. **81**, 3440 (1997)
30. K. Behler, S. Osswald, H. Ye, S. Dimovski, Y. Gogotsi, J. Nanopart. Res. **8**, 615 (2006)